

Research Article

Open Access

Bruno Giovanni*, Carucci Fabrizio

2D numerical analysis of the seismic response of a karst rock mass: importance of underground caves and geostructural details

<https://doi.org/10.2478/sgem-2019-0028>
received April 12, 2019; accepted August 21, 2019.

Abstract: The present study shows the results of a 2D local seismic response (LSR) analysis, simulated for a geomechanical model consisting of a layered carbonate rock mass with hypogean karst caves and a structural–lithostratigraphic complex setting, in an area within the Municipality of Turi (Apulia, Italy). In this case study a Distinct Element Code (DEM) code (UDEC) was used for the LSR simulations conducted on a model both in the absence and in the presence of two overlapping karst caves. The preliminary stress–strain model analysis show some tensile yielding points clustered on the roof of the upper karst cave, already in static conditions, and the phenomenon becomes even more noticeable in dynamic conditions. This is perfectly in agreement with the real occurrence of a sinkhole that brought to the light the underlying karst cave, in the case study area, in the recent past.

The amplification/deamplification factor (FA) was calculated as the ratio of the top value to the bottom value in the model, both of the max X-acceleration and of the spectral Fourier amplitude in three different ranges of frequencies, in order to estimate the effects of LSR on the X-component of the seismic input. According to the previous studies, the results obtained show a generalised deamplification of the seismic ground motion at the top of the model, both without and with underground karst caves, caused by the presence of the upper karst cave and by the seismic energy absorption because of layers' discontinuity.

Keywords: 2D local seismic response analysis, rock mass, karstic underground caves

1 Introduction

The presence of discontinuities and faults inside a rock mass has a significant influence on the way of propagation of seismic waves and on their amplification effects on the ground level [1] [2]. The situation will further complicate if one or more underground caves (anthropogenic or natural) are present in the rock mass [3], [4], [5], [6], [7]. The site effect evaluation appears to be complex because of these conditions, so that it cannot be conducted with one-dimensional numerical code. On the contrary, two-dimensional or three-dimensional software, such as UDEC [8], are more appropriate to conduct this kind of analysis because it is possible to model both the presence of an underground cave and the discontinuous and anisotropic characteristics of the geotechnical model. Previous studies mainly referred to models with homogeneous and isotropic rocks, without considering rock mass with faults and underground karstic caves. The local seismic response (LSR) analysis of these models (especially in the professional practice) is usually conducted on 1D models, in which only the stratigraphic variation is considered. In the past few years, studies on LSR have been increasing significantly in literature. They aim to evaluate the influence of reliefs, valleys, faults and underground caves [3], [4], [5], [6], [7], [9], as well as the soil–structure interaction [10], [11]. However, even more recent studies are based on homogeneous and isotropic subsoil models and are mainly conducted with finite element method (FEM), finite difference method (FDM), and boundary element method (BEM) calculation software which are not suitable in the case of discretely fractured and/or stratified rock masses, unlike the discontinuous deformation analysis (DDA) [12], [13] and distinct element method (DEM), the latter used in the present case study [14],

*Corresponding author: Bruno Giovanni, Politecnico di Bari, Department of Civil, Environmental, Land, Building Engineering and Chemistry, via Orabona 4, 70125 Bari, Italy, E-mail: giovanni.bruno@poliba.it
Carucci Fabrizio, Equienergia s.r.l., Via Domodossola 3, 20145 Milano, Italy

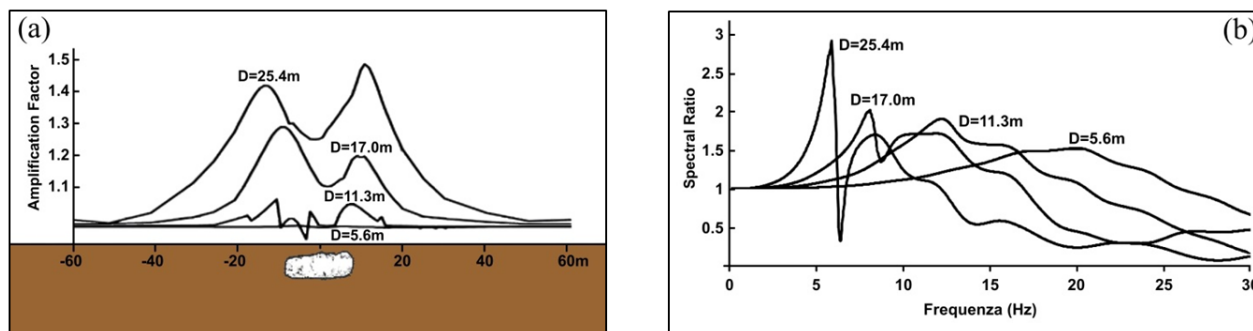


Figure 1: Amplification factor (a) and spectral ratio (b) values above an underground cave inside a homogeneous and isotropic subsoil crossed by V_s waves, based on the parametric variation of the cave diameter (from [7] modified).

[15]. Studies about LSR on real and/or parametric cases [6], [7] were conducted on homogeneous and isotropic subsoil, varying the diameter and the depth of the cave. These studies highlighted the strong influence of these two variables over the amplification factor (FA), mostly in the frequency domain (Fig. 1). Overall, a decrease in the FA factor is observed as the cave depth (H) increases and, considering the same depth, as the cave diameter (D) decreases. Moreover, previous studies underline that diameter's influence on LSR decreases dramatically for $D \leq 5.6$ m, that is, for diameters comparable to case study. Furthermore, the effects of amplification/deamplification of the ground motion above a cave are significantly different, depending on whether the V_p or V_s volume waves hit the cave. In the case of V_s waves, the amplification effects on the surface are concentrated on the cave sides, while a deamplification occurs above the cavity. On the other hand, in the case of V_p waves, the amplification of the ground motion is concentrated at the centre of the cavern and decrease sharply, moving to its boundaries.

The UDEC numerical program was used to simulate the LSR of an anisotropic and discontinuous geotechnical model of a real case study, in order to analyse the effects of the simultaneous presence of underground caves, discontinuities and lithostratigraphic variations.

2 Geostructural and morphological layout of the area

The case study area is part of the extensive Apulian karst area of the Murge. In particular, it is located in the northwest neighbourhood of the town of Turi (Bari, Italy). From the geological and stratigraphic point of view, the rocks that constitute the substratum can be traced back to the

'Calcari di Bari' Mesozoic formation. This is a succession of whitish micritic limestones, dolomite limestones and greyish dolomite with local small inclusions and/or grey leading to black coloured laminations (Fig. 2). These limestones have a thickness of several hundred metres. In the study area, they are stratified with layers of 1-m thickness (standard deviation, 0.5 m), position $D = 330^\circ$, $i = 5^\circ$ (standard deviation, 1°) and $I = 60^\circ$. The tectonic structures found in the area are attributable to two phases, characterised by different tension fields. The first phase had a compressive nature and generated a smooth anticlinal fold, whose axis are oriented approximately northwest–southeast. The fold lies a few hundred metres south of the study area which is, therefore, placed on the northeast side of this anticline. On the other hand, the second phase generated two normal faults defining a small graben, with northeast–southwest oriented axis, in which the case study area falls.

However, it must be said that the two normal faults are not directly detectable on the surface, as they are interformational and with minimal vertical component of dip-slip.

Their location and orientation stemmed from the correlations between the stratigraphic reconstruction through different borings performed and the electrical tomographies acquired from previous studies. An ephemeral watercourse has set itself, with a south south east - north north west course, along the tectono-karstic depression of the graben, which is locally named as 'lama'. This depression plays a role in drainage and vehiculation of rainwater. However, the water flow occurs underground (and not on the surface), because of the lithological nature of the rocks in the area and their high permeability (because of fracturing and karst), especially in the most superficial layers of the rock mass. As a result of the carbonatic nature of the rock mass, the landscape

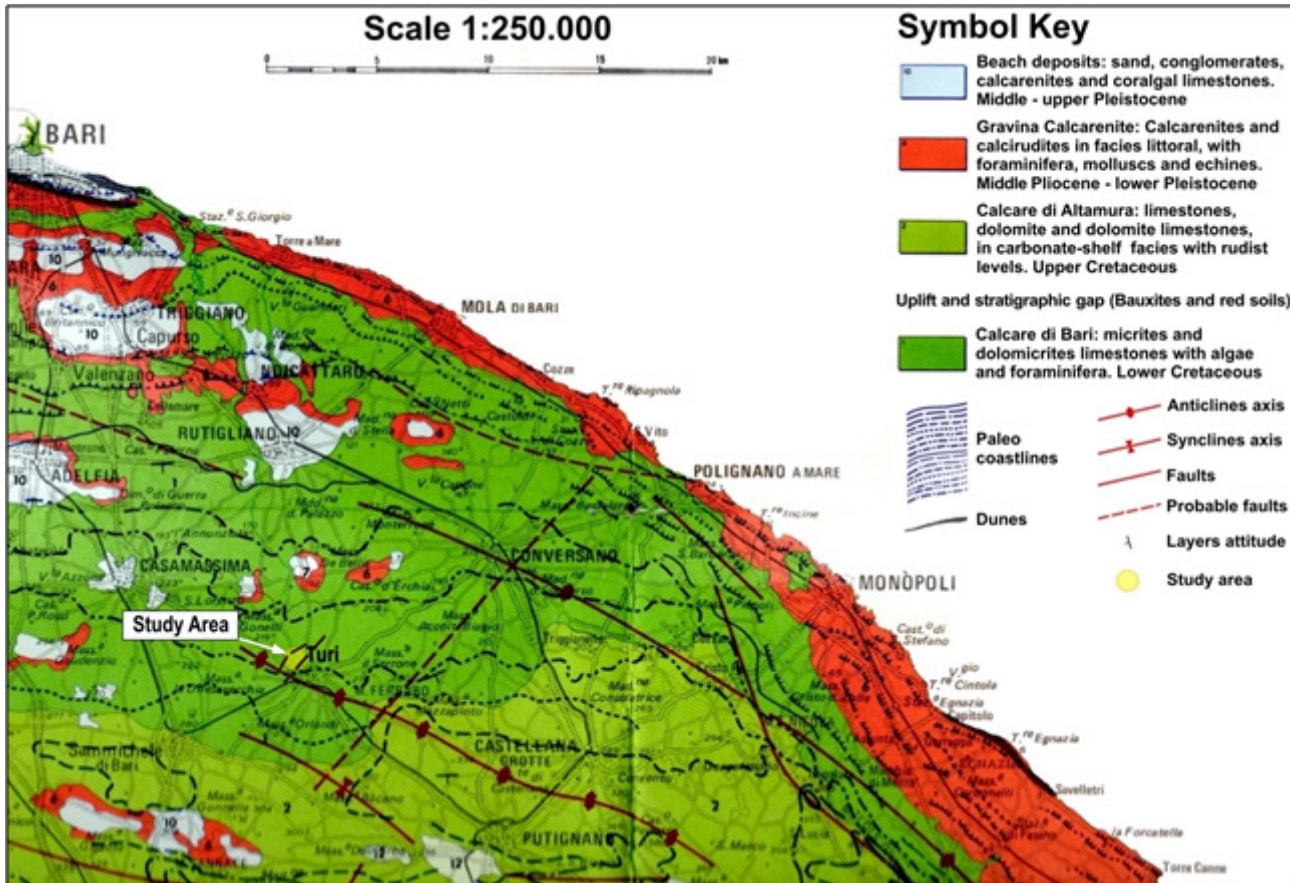


Figure 2: Geological map of the territory in which the study area is located (from [16] modified).

morphology of the area is essentially related to the karst phenomenon. It manifests itself both with epigeal morphologies, such as the dolina located mostly south of the study area, and with hypogean morphologies, such as the sinkhole ‘capovento’ located at the west side of the ‘Don Bosco’ nursery school. Other hypogean karst forms have been found a few hundred metres to north north east from the study area, such as the cave of ‘S. Oronzo’ and an adjacent small cave located a few decimetres underneath the surface.

3 In situ investigation and geomechanical model of the rock mass

The widespread presence of underground karst caves in the Murge area, the proximity of the S. Oronzo’s cave and the structural arrangement of the area suggest that the ‘capovento’ sinkhole is not isolated, but connected to an underground karstic cavern. This assumption is

supported by resistivity values found in previous indirect investigations, provided by the technical department of the municipality of Turi (BA), such as electric tomographies with Wenner–Schlumberger arrays (Fig. 3).

The analysis of the n.1 tomography (the most representative one) showed a low resistivity anomaly, flanked by high resistivity areas, beneath the sinkhole ‘capovento’. The trend of resistivity is confirmed by the graben structural layout, in the centre of which the karstic sinkhole ‘capovento’ develops. The normal faults, positioned on the sides of the graben, are identified by the sharp contrast between high resistivity values on the sides and low values in the centre. Finally, low resistivity values can be explained by two evidences. The first one is the underground water circulation, which is channelled along the tectono-karstic depression ‘lama’, at a depth of about 10–14 m from the surface, along directives from southeast to northwest. The second one is the possible presence of underground karst caves filled with residual clay, known in the area as ‘red soils’. Mechanical surveys, with continuous core drilling and core destruction, were performed with the purpose of clearly identifying the

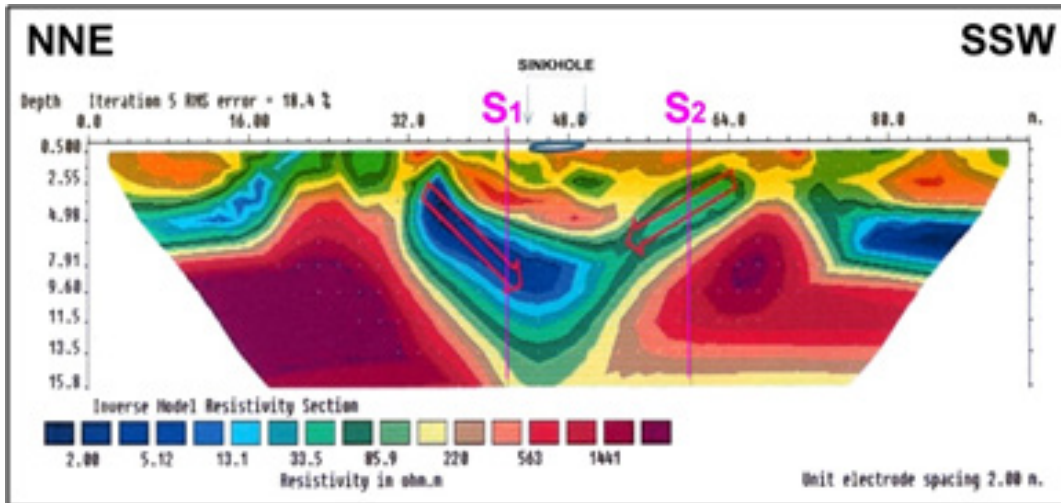


Figure 3: Electric tomography n.1: resistivity values and projection of cores drilling S1 and S2 (from Technical Department of the municipality of Turi (BA) – modified).

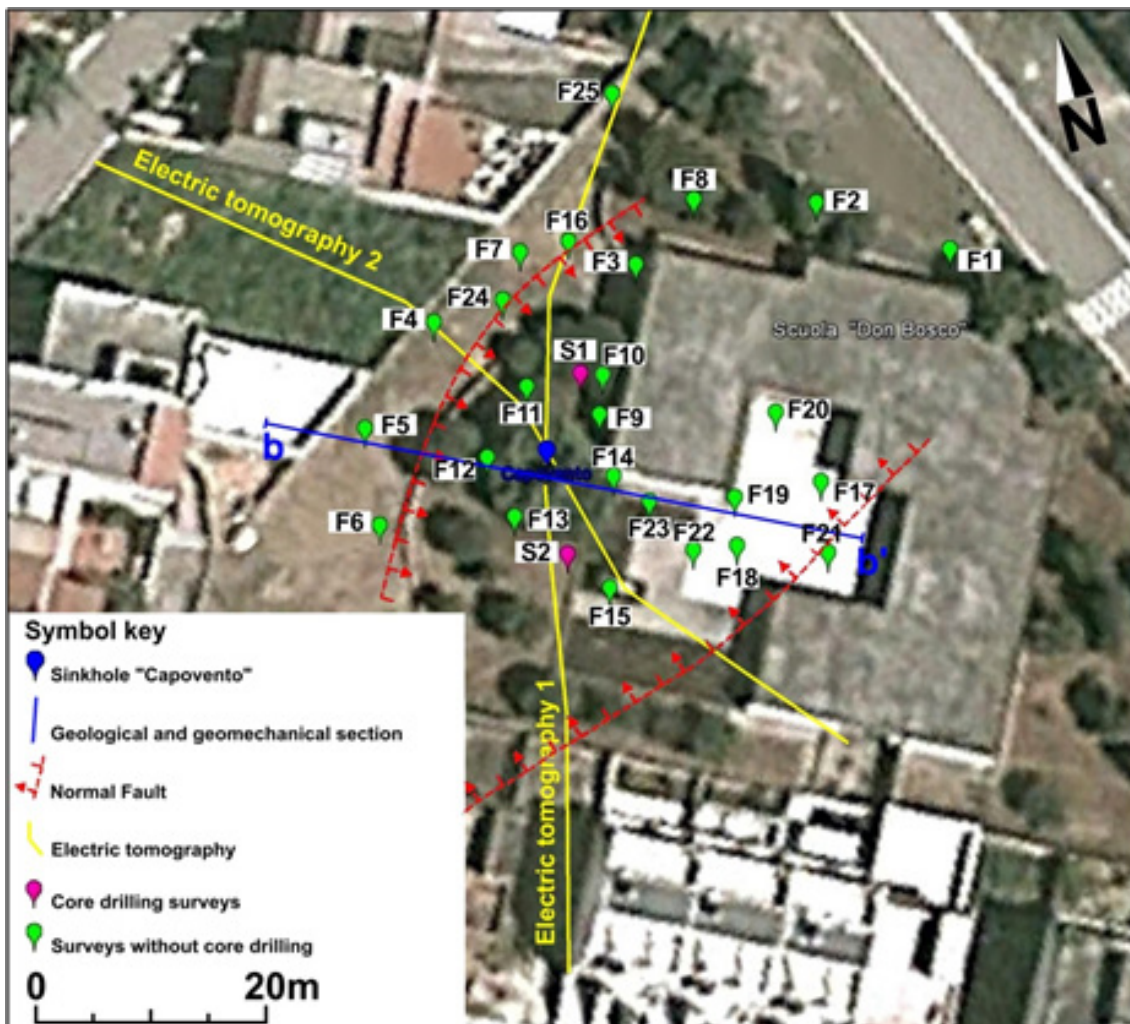


Figure 4: Location of geological surveys and section of the geological and geomechanical model.

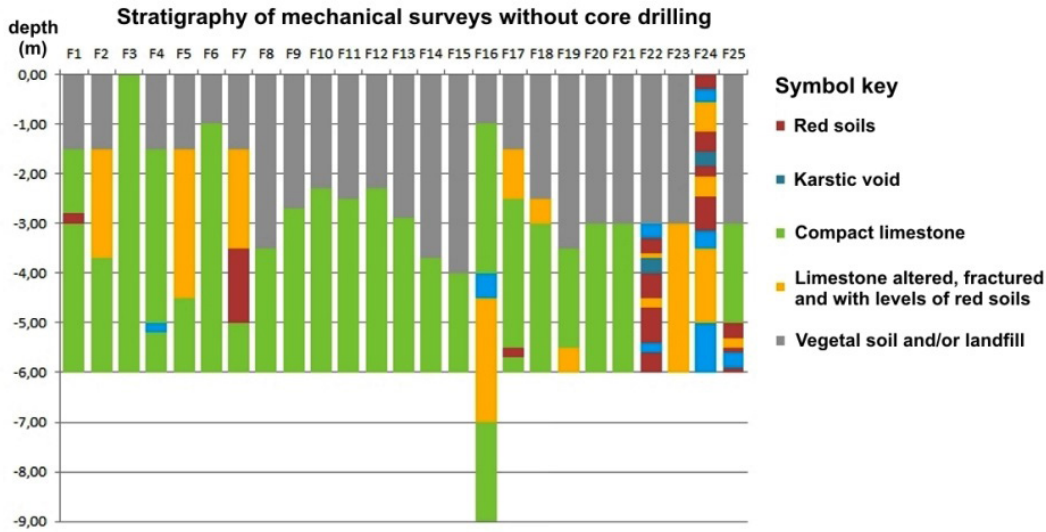


Figure 5: Stratigraphy obtained from the core destruction borings.

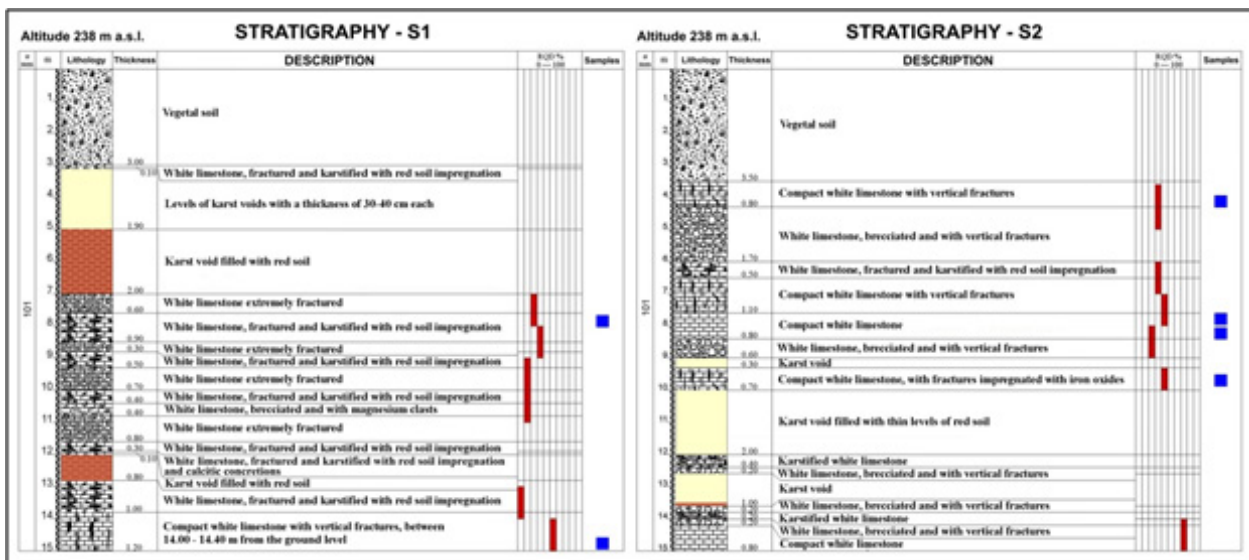


Figure 6: Stratigraphies obtained from rotation drills with continuous coring, RQD trend along verticals and depth of the rock samples for geotechnical laboratory tests.

presence of a karstic cave connected to the sinkhole and to potentially reconstruct its geometry (Fig. 4).

In particular, 25 core destruction borings (diameter $\Phi = 60$ mm and depth of 6 m from the ground level) and 2 rotation drills with continuous coring (diameter $\Phi = 101$ mm and depth of 15 m from the ground level) were performed. Both the core destruction borings and the rotation drills with continuous coring had the purpose of finding the hypogean caves and determining their geometric extension (Fig. 5). Moreover, those with continuous coring have allowed to collect six samples for geotechnical tests

(two in the S1 core drill and four in the S2 one) and to evaluate the rock quality designation (RQD) index and its variation along boring verticals (Fig. 6). Furthermore, the planimetric and altimetric characteristics of the nearby S. Oronzo’s cave were considered for the reconstruction of the geometry of the hypogean caves, which have been identified with the geological surveys.

The S. Oronzo’s cave, indeed, is a karstic one of interlayer type with a planimetric development (91.00 m), which is predominant compared to the altimetric one (20.50 m). Besides, it is articulated on two overlapping

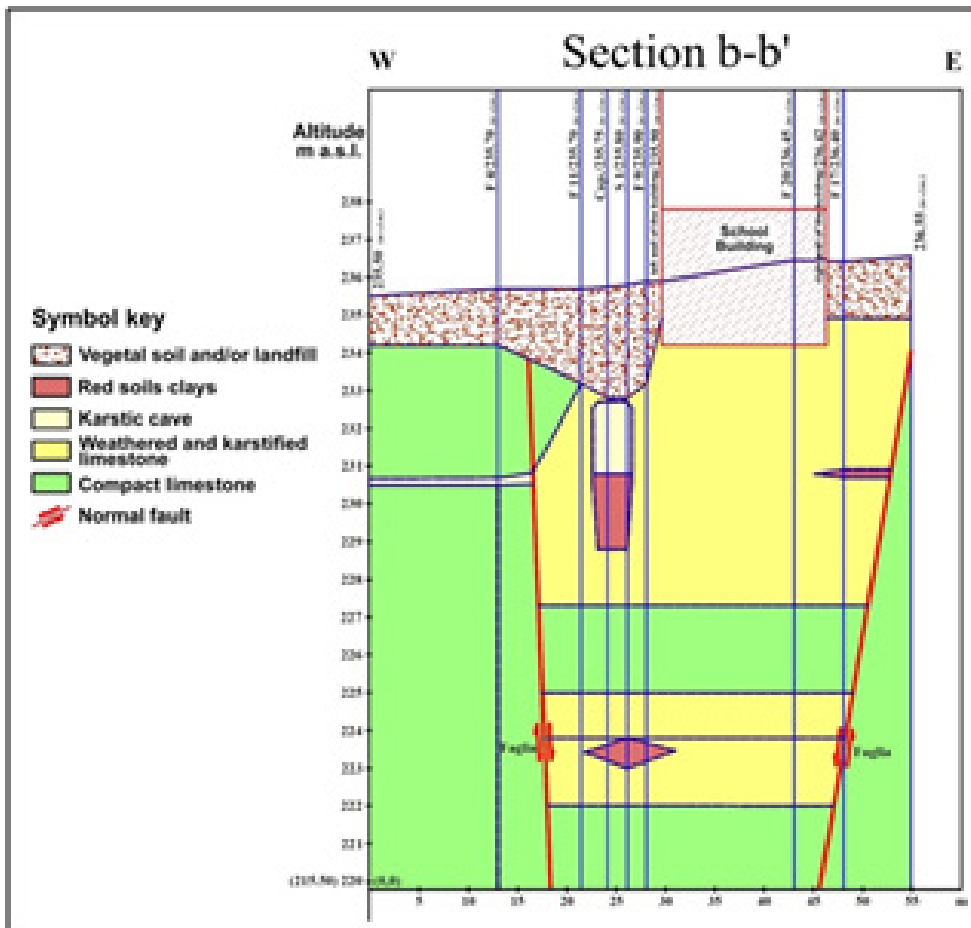


Figure 7: Geomechanical model section used for the LSR evaluation; the upper karst cave has a height of $L = 4.00$ m and a width of $D = 3.00$ m.

karst levels. The deepest level, northwest–southeast oriented, presents cave bottom altitudes between 215.50 and 209.50 m a.s.l., while the more superficial one, oriented north–south and northwest–southeast, presents cave bottom altitudes between 218.00 and 214.00 m a.s.l.

Also, the cave connected to the vertical sinkhole ‘capovento’, adjacent to the ‘Don Bosco’ nursery school, is of the interlayer type, with a prevalently sub-horizontal development on two overlapping karst levels. The development direction of the deepest level is from SE to NW, with a total height of about $L = 1.50$ m and cave bottom altitudes between 226.90 and 222.30 m a.s.l. The most superficial karst level consists of two ramifications that start from the sinkhole ‘capovento’ and develop one in the northwest direction and the other in the north north east direction. The cave has a height of about $L = 4.00$ m in correspondence with the sinkhole ‘capovento’ and barely more than $L = 1.00$ m in correspondence of the two branches that start from it; moreover, the altitudes of

the cave bottom are between 225.20 and 234.90 m a.s.l. In the geomechanical model section, used for the LSR evaluation, the compact and not altered limestone was distinguished from the altered and karstic one, depending on the alteration level and the karst increase (Fig. 7).

Considering that the numerical code used for the LSR analysis is a DEM one [8], [14], [15], [17], [18], it was necessary to parameterise the geomechanical model. Therefore, laboratory tests on the six specimens taken from the mechanical borings (conducted at the ‘M. Salvati’ laboratory–DICAR Department, Politecnico di Bari) and geomechanical measurement in situ were conducted. The collected data allowed to classify the rock mass with the Bieniawski RMR’76 indexes [19] and to estimate the friction angle and the cohesion values. Moreover, the GSI values were obtained (Table 1) through the correlations between the geomechanical classification indexes [20], [21]:

$$\text{GSI} = \text{RMR}'76 \text{ (valid when RMR}'76 \geq 18)$$

Table 1: Geomechanical classification of the altered and the compact calcareous rock mass.

	Parameters	Values	RMR ₇₆	GSI
Rock mass Altered and karstic limestone	R ₁ (compressive strength)	7	49	φ _b = 35° c _b = 0.15 MPa
	R ₂ (RQD)	6		
	R ₃ (spacing of discontinuities)	15		
	R ₄ (joint conditions)	11		
	R ₅ (water conditions)	10		
Rock mass Compact and not altered limestone	R ₁ (compressive strength)	7	62	φ _b = 40° c _b = 0.20 MPa
	R ₂ (RQD)	13		
	R ₃ (spacing of discontinuities)	15		
	R ₄ (joint conditions)	17		
	R ₅ (water conditions)	10		

Table 2: Mechanical parameters of rocks and discontinuities (based on laboratory tests) of the geomechanical model.

VEGETAL SOIL AND “RED SOILS”							
r	E	v	K	G	φ	c	σ _i
(Kg/m ³)	(Pa)		(Pa)	(Pa)	(grade)	(Pa)	(Pa)
1835	20·10 ⁶	0.25	13·10 ⁶	8·10 ⁶	25	50000	0

ALTERED AND KARSTIC LIMESTONE from laboratory tests						ALTERED ROCK MASS from Hoek-Brown linearized criterion				
r	σ _{ci}	σ _{ti}	E	v	K	G	φ _b	c _b	σ _{tb}	σ _{cb}
(Kg/m ³)	(Pa)	(Pa)	(Pa)		(Pa)	(Pa)	(grade)	(Pa)	(Pa)	(Pa)
2345	58·10 ⁶	7·10 ⁶	4·10 ¹⁰	0.20	22·10 ⁹	17·10 ⁹	40	0.4·10 ⁶	0.2·10 ⁶	3·10 ⁶

COMPACT AND NOT ALTERED LIMESTONE from laboratory tests						COMPACT ROCK MASS from Hoek-Brown linearized criterion				
r	σ _{ci}	σ _{ti}	E	v	K	G	φ _b	c _b	σ _{tb}	σ _{cb}
(Kg/m ³)	(Pa)	(Pa)	(Pa)		(Pa)	(Pa)	(grade)	(Pa)	(Pa)	(Pa)
2345	69·10 ⁶	8·10 ⁶	6·10 ¹⁰	0.20	33·10 ⁹	25·10 ⁹	50	1·10 ⁶	0.4·10 ⁶	8·10 ⁶

DISCONTINUITY – ALTERED AND KARSTIC LIMESTONE				
jk _n	jk _s	φ	c _j	σ _{ti}
(Pa/m)	(Pa/m)	(grade)	(Pa)	(Pa)
1·10 ⁹	1·10 ⁸	30	0.4·10 ⁶	0

DISCONTINUITY – COMPACT AND NOT ALTERED LIMESTONE				
jk _n	jk _s	φ _j	c _j	σ _{ti}
(Pa/m)	(Pa/m)	(grade)	(Pa)	(Pa)
1.2·10 ⁹	1·10 ⁸	35	0.4·10 ⁶	0

NORMAL FAULT				
jk _n	jk _s	φ _j	c _j	σ _{ti}
(Pa/m)	(Pa/m)	(grade)	(Pa)	(Pa)
1.2·10 ⁹	1·10 ⁸	60	0.4·10 ⁶	0

Table 3: Relevant input data for the accelerograms search with the REXEL 3.5 software.

Target Spectrum	a_g (g)	Geographic Coordinates ED50		Site class	Topographic category	Nominal Life	Functional Type	Limit State	M	R (km)
		Lat. N	Long. E							
Italian Building Code 2008	0.074	17.0222	40.9185	A	T1	50 years	III	SLV	6-7	0-100

Table 4: Main data of the seismic events extracted from the database for the X-acceleration (above) and the Z-acceleration (below).

Waveform ID	Earthquake ID	Station ID	Earthquake Name	Date	Mw	Fault Mechanism	Epicentral Distance (km)	EC8 Site class
286	146	ST92	Campano Lucano	11/23/1980	6.9	normal	78	A

Waveform ID	Earthquake ID	Station ID	Earthquake Name	Date	Mw	Fault Mechanism	Epicentral Distance (km)	EC8 Site class
172	81	ST48	Basso Tirreno	04/15/1978	6	oblique	58	A

In addition, the Hoek–Brown curvilinear strength criterion [20] was implemented using the values of the mechanical parameters obtained from the laboratory tests and the GSI classification indexes. This criterion considers the strong non-linearity of the strength envelope, which is typical of the rock masses, and estimates the representative parameters, even by means of the Mohr–Coulomb linearisation. The physical–mechanical parameters used for the rocks and the discontinuities of the geomechanical model are summarised in Table 2.

4 Seismic characterization of the case study area and choice of the seismic input

In order to assess the LSR of the case study, the seismic input consists of two accelerograms, respectively, for the X-component and Z-component of seismic input motion. Therefore, according to the seismic hazard of the case study area (Table 3) and the Technical Standards for Italian Constructions (Norme Tecniche per le Costruzioni Italiane [23]), the accelerograms were extracted from the European Strong-motion Database [24] [25] present in the REXEL 3.5 software [26].

These accelerograms are natural and spectrum compatible; moreover, the focal mechanism (normal

fault) and the bedrock lithology (carbonatic rocks) were compatible with those of the case study area (Table 4).

Subsequently, the accelerograms previously extracted, which are the most spectrum-compatible and also those that have a scale factor closer to the average value (SF_{mean}) of the respective combinations of seven earthquakes, were processed with SeismoSignal software [27] to obtain the X-velocity and Z-velocity which were used to define the seismic input for the UDEC numerical simulation (Fig. 8). The seismic waves velocities $V_s = 2821$ m/s and $V_p = 4607$ m/s in the rock mass were inferred from previous seismic refraction traverse, provided by the technical department of the municipality of Turi (BA).

5 2d distinct elements numerical static and dynamic analysis

To evaluate the LSR of the case study, two discontinuous models with deformable blocks were designed using the UDEC2D distinct element numerical code. The constitutive model used for rock blocks, discontinuities and faults was the Mohr–Coulomb plasticity one. This model was chosen both because it is one of the most efficient computationally plasticity models and the analysis concerns general rock mechanics issues (e.g. slope stability and underground excavation). Before starting the dynamic analysis, aimed

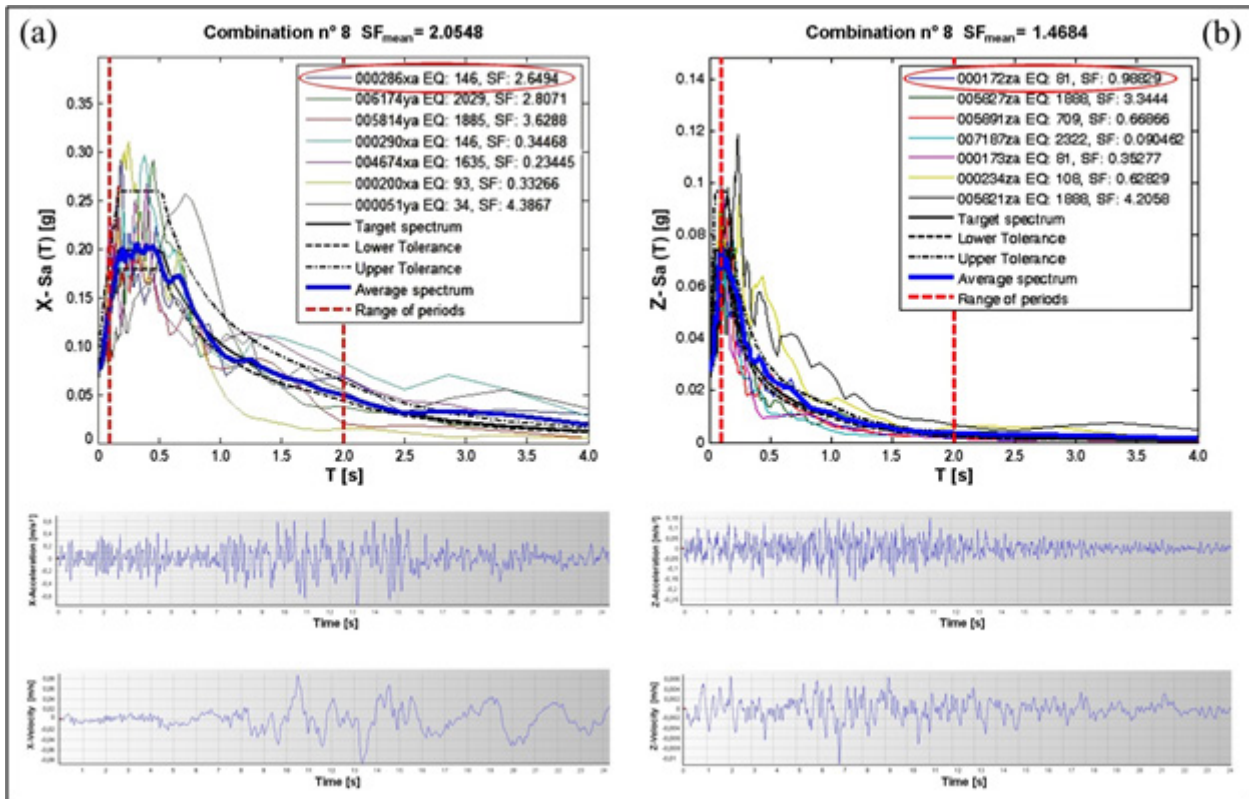


Figure 8: Acceleration–period spectra of the combinations no 8 and accelerogram/velocity time–history of the two earthquakes chosen (red circled) for the LSR analysis: X-component (a) and Z-component (b).

at the LSR evaluation, it was crucial to properly define the boundary conditions and the calculation options:

- presence of a ‘graben’ adjacent to the school building and within which the two overlapping underground caves are located;
- presence of a tectono-karstic palaeochannel ‘lama’, located above the underground caves and flanked by the school building, filled by vegetal soil and/or landfill with a maximum thickness of 3-m;
- loads transmitted by the school building foundation (isolated plinth type) on the substratum;
- use of viscous boundaries at the base of the model and on the three sides of the foundation excavation and free field conditions on the sides of the model;
- Rayleigh damping equal to 5% of the critical damping, applied to the natural vibration frequency of the system;
- seismic waves incidence angle $\theta = 0^\circ$;
- seismic waves velocity $V_s = 2821$ m/s and $V_p = 4607$ m/s in the rock mass.

The static stress-deformation analysis of the rock mass showed that the model has tensile plasticisation points

that tend to cluster on the roof of the upper karst cavity (Fig. 9). These yielding conditions, accompanied by downward displacements of the rock blocks of the karst cavity roof, are even more evident in the results of the dynamic analysis.

6 The local seismic response of the case study model

According to previous studies [9], [10], and general considerations described above, the LSR simulation of the case study was finally assessed considering two hypotheses: the absence and presence of the two overlapping karst caves. For the simulation, the model was extended for a length of 25–30 m on both the sides of karst caves, the boundary conditions listed above were applied and, in addition, 18 control points were placed, 9 at the base of the model, and the others 9 (aligned with the first ones) on the ground level (Fig. 10). The amplification/deamplification (FA) and the most amplified frequencies on the ground level of the model were analysed to estimate

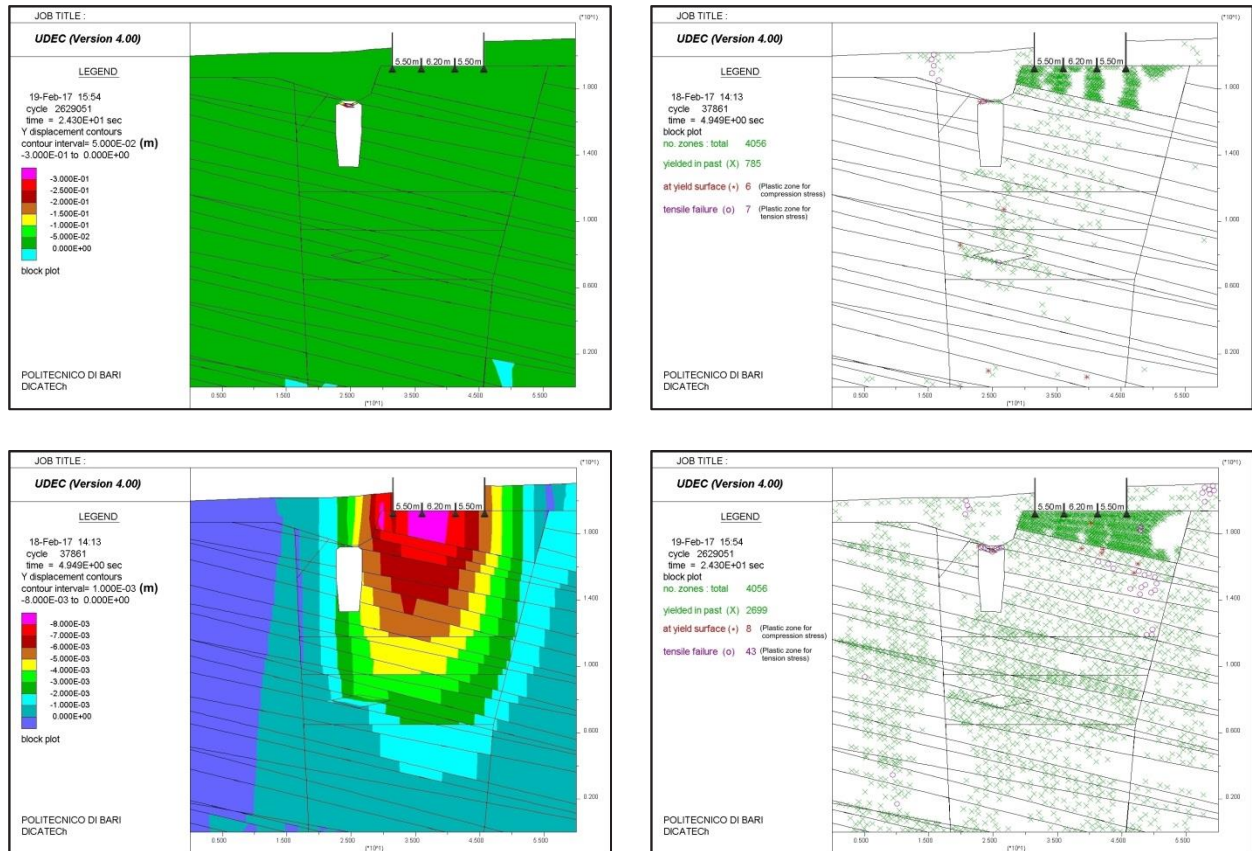


Figure 9: Trend of displacements in the Y-direction (left) and plastic zones (right) in the geomechanical model with two overlapping underground caves: in static (above) and dynamic (below) conditions.

the effects of LSR on the X-accelerations component. More specifically, in each control point on the ground level of the model, the amplification/deamplification (FA) has been calculated using two methods (Table 5):

a) ratio between the values of the maximum X-acceleration (A_{Xmax}) in the points at the top of the model and in the corresponding ones at the base [9], [10];

b) ratio between the values of the Fourier's amplitudes spectrum in the points at the top of the model and in the corresponding ones at the base for three ranges of frequencies normally used in previous RSL studies [10], [11]: 0.2–2.0, 2.0–3.8 and 3.8–5.6 Hz. These frequencies are comparable with the computed natural ones of the existing buildings in the case study area, ranging roughly between 2.21 and 3.10 Hz.

The maximum values of FA, for both the calculation hypotheses (with or without the caves) and for the two calculation methods implemented, are found on the right edge of the caves at no. 8 control point, close to the edge of the school building foundations (Fig. 10).

Furthermore, the FA values obtained with both calculation methods showed that, in general, in the control points at the ground level of the model, there is a deamplification of the seismic motion (Table 5). The only exception is represented by the point no. 8 in the hypothesis without caves, where the FA = 1.672 (ratio between the max X-accelerations) would highlight a local effect of seismic amplification. Furthermore, between the three frequency ranges analysed in the simulations, those that are most amplified are 2.0–3.8 Hz (without caves) and 3.8–5.6 Hz (with caves).

Finally, it should be observed that the UDEC dynamic analysis is conducted with a linearly elastic behaviour of the rocks. The values of the seismic FA on the ground level of the model are, therefore, lower or at the most equal to those that would be obtained with a non-linear analysis, because the degradation of the stiffness and shear modules of the rocks, especially of the vegetal and/or landfill soil, increases the seismic amplification on the ground level [2], [15].

Table 5: FA, calculated in the absence and presence of karst caves, as ratio of the maximum X-acceleration and ratio of the Fourier’s amplitudes spectrum in three ranges of frequency.

Output Point ID	$\frac{A_{Xmax.Top}}{A_{Xmax.Bottom}}$		$\frac{\int_{0.2Hz}^{2.0Hz} Fourier\ Ampl.Top(f)}{\int_{0.2Hz}^{2.0Hz} Fourier\ Ampl.Bottom(f)}$		$\frac{\int_{2.0Hz}^{3.8Hz} Fourier\ Ampl.Top(f)}{\int_{2.0Hz}^{3.8Hz} Fourier\ Ampl.Bottom(f)}$		$\frac{\int_{3.8Hz}^{5.6Hz} Fourier\ Ampl.Top(f)}{\int_{3.8Hz}^{5.6Hz} Fourier\ Ampl.Bottom(f)}$	
	Without caves	With caves	Without caves	With caves	Without caves	With caves	Without caves	With caves
	1	0.060	0.033	0.067	0.039	0.072	0.033	0.065
2	0.084	0.221	0.120	0.043	0.122	0.097	0.118	0.070
3	0.012	0.129	0.161	0.090	0.176	0.048	0.171	0.040
4	0.730	0.036	0.161	0.090	0.176	0.048	0.171	0.040
5	0.048	0.009	0.098	0.071	0.123	0.040	0.119	0.053
6	0.169	0.057	0.079	0.035	0.113	0.021	0.142	0.024
7	0.093	0.024	0.079	0.035	0.113	0.021	0.142	0.024
8	1.672	0.899	0.259	0.272	0.274	0.172	0.236	0.342
9	0.120	0.019	0.093	0.058	0.143	0.052	0.084	0.113

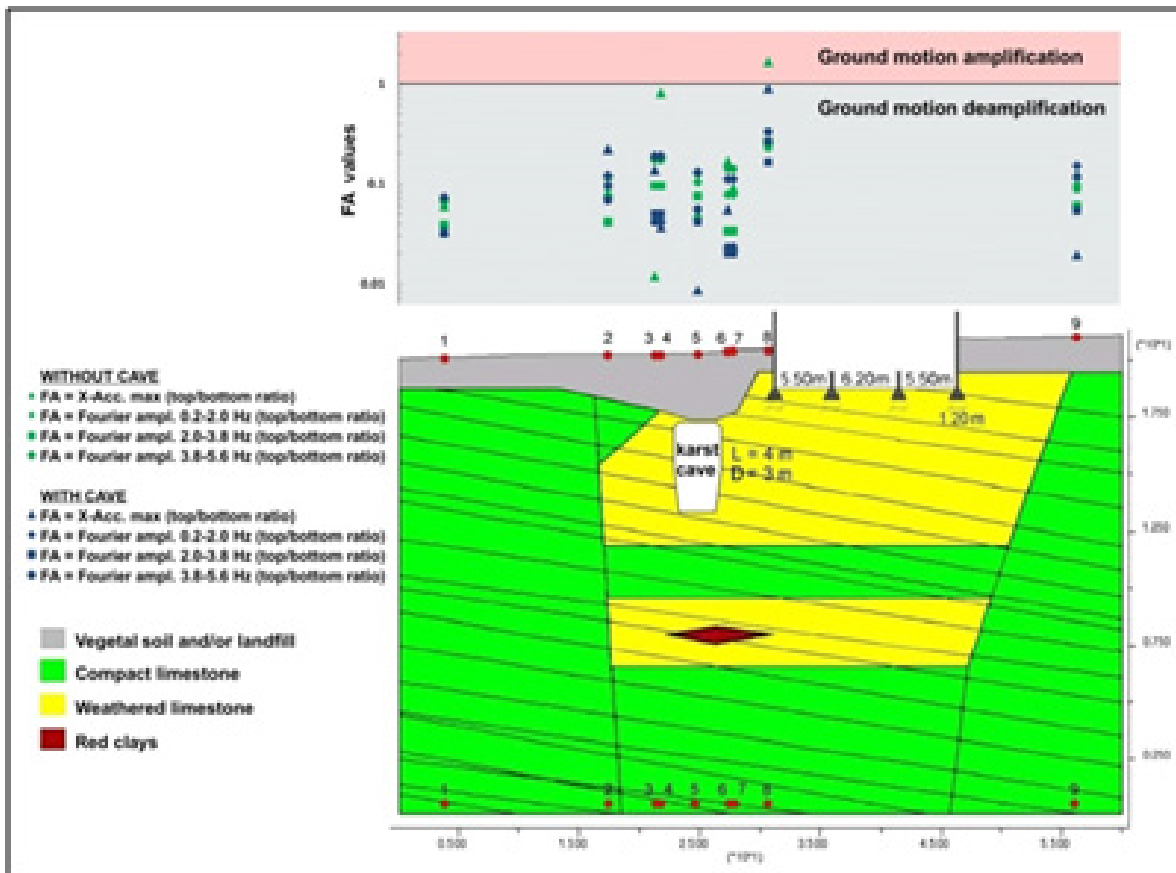


Figure 10: LSR amplification/deamplification, as X-accelerations FA, in each of the control points at the ground level of case study model.

7 Concluding remarks

Preliminarily to the case study LSR, the stress–strain analysis of the rock mass (Fig. 9) showed that the model presents, already in static conditions, but even more in dynamic ones, tensile plasticisation points that tend to cluster on the roof of the upper karst cavity. Moreover, in dynamic conditions, the downward displacements of the rock blocks of the karst cave roof are compatible with a local collapse of the same. The results of the modelling are in perfect agreement with the real occurrence of a sinkhole that, in the recent past, brought to the light the underlying karst cave in the case study area.

The LSR numerical simulation evaluated by the values of FA obtained with two distinct calculation methods shows a generalised deamplification of seismic motion on the ground level of the model, both in the absence and in the presence of hypogean karst caves. The only exception to this trend is represented by point no. 8 in the hypothesis without caves, where an FA = 1.672 (ratio between the max X-accelerations) should highlight a local effect of seismic amplification. The presence of the lower karst cave, filled by ‘red soils’ clay, and the thin vegetal soil that fills the paleochannel ‘lama’ do not seem to influence the model’s LSR.

The generalised deamplification for the horizontal component of the ground level seismic motion is in agreement with what was reported in the previous studies [1], [15], [28] about the relevant effect of seismic energy absorption operated by the layer discontinuities. Moreover, the effect of seismic deamplification at the top and in axis with the underground caves, already highlighted in the literature for cavities with diameter $D > 5.6$ m in homogeneous and isotropic substrate models [7], is confirmed by the minimum FA values reached at the point no. 5, with both calculation methods, even for a cave with $D < 5.6$ m.

Acknowledgment: Thanks to the Municipality of Turi for having made available the previous geophysical data and for the authorisation to publish the results of this research.

References

- [1] Pyrak-Nolte L. J., Myer L. R., Cook Neville G. W. - Transmission of Seismic Waves Across Single Natural Fractures. *Journal of Geophysical Research*, vol. 95, n° B6, 8617-8638, June 10, 1990.
- [2] Ghosh A., Hsiung S. - Effects of tilted and faulted strata on seismic ground motion. U.S. Nuclear Regulatory Commission Contract NRC-02-07-006, Center for Nuclear Waste Regulatory Analyses, San Antonio, Texas, 2011.
- [3] Rodriguez-Castellanos A., Sánchez-Sesma F. J., Luzón F., and Martin R. - Multiple scattering of elastic waves by subsurface fractures and cavities. in *Bulletin of the Seismological Society of America*, vol. 96, n. 4A, 1359-1374, 2006.
- [4] Smerzini C., Avilés J., Sánchez-Sesma F. J., and Paolucci R. - Analytical solutions for the seismic response of underground structures under SH wave propagation. *AIP Conference Proceedings* 1020, 674, <https://doi.org/10.1063/1.2963900>, 2008.
- [5] Smerzini C., Avilés J., Paolucci R. and Sánchez-Sesma F. J. - Effect of underground cavities on surface earthquake ground motion under SH wave propagation. in *Earthquake Engineering and Structural Dynamics*, n.38, 1441-1460, 2009.
- [6] Verrucci L, Lanzo G, Pagliaroli A, Sano` T. - Effects of cavities on seismic ground response. In: *Proceeding. Second international conference on performance-based design in earthquake geotechnical engineering*, May 28-30 2012, Taormina (Italy), CDROM, paper #1.15, 2012.
- [7] Sanò T. - Risposta sismica locale in aree con presenza di cavità. in *Geologia dell’Ambiente - Supplemento al n.2/2013*, 55-61, 2013.
- [8] Itasca Consulting Group, Inc. “UDEC Version 4.0 User’s Guide.” Minneapolis, Minnesota: Itasca Consulting Group, Inc. 2011.
- [9] Scotto di Santolo A., de Silva F., Calcaterra D., Silvestri F. - Site effects due to the presence of cavity near the cliffs. 6th International Conference on Earthquake Geotechnical Engineering 1-4 November 2015 Christchurch, New Zealand, 2015.
- [10] Evangelista L., Landolfi L., d’Onofrio A., Silvestri F. - The influence of the 3D morphology and cavity network on the seismic response of Castelnuovo hill to the 2009 Abruzzo earthquake. *Bulletin of Earthquake Engineering*, 14, 3363-3387, DOI: 10.1007/s10518-016-0011-8, 2016.
- [11] Piro A., de Silva F., Parisi F., Silvestri F., Scotto di Santolo A. - Interazione sismica tra terreno, cavità e struttura: un caso di studio nel centro storico di Sant’Agata de’ Goti. XXVI Convegno Nazionale di Geotecnica, Rome, Italy, June 2017.
- [12] Fu X., Sheng Q., Zhang Y., Chen J., and Leng X. - Extension of the discontinuous deformation analysis method to simulate seismic response of a large rock cavern complex. *Int. J. Geomech.*, 17(5):E4016008, DOI: 10.1061/(ASCE)GM.1943-5622.0000712, (2016b).
- [13] Hsiung S. M., Shi G. H. - Simulation of earthquake effects on underground excavations using discontinuous deformation analysis (DDA) [A]. In: *Rock Mechanics for Industry [C]*, 1413-1420, 1999.
- [14] Ahola M.P., Chowdhury A.H. - Effect of seismic load on a proposed nuclear waste repository at Yucca Mountain. *Inter. Jour. of Rock Mech. and Min. Science*, 34 (3-4), ISSN 0148-9062, 1997.
- [15] Barla G., Monacis G., Perino A., Hatzor Y. H. - Distinct Element Modelling in Static and Dynamic Conditions with Application to an Underground Archaeological Site. *Rock Mechanics and Rock Engineering*, 43 (6), 877-890, 2010.
- [16] Ciaranfi N., Pieri P., Ricchetti G. - *Carta Geologica delle Murge e del Salento*. Mem. Soc. Geol. It., 42, 1988.
- [17] Cundall P.A., Hart R. D. - Development of generalized 2-D and 3-D distinct element programs for modeling jointed rock. Itasca

- Consulting Group, U.S. Army Corps of Engineers, Misc. Paper SL-85-1, 1985.
- [18] Marcato G., Silvano S., Zabuski L. - Modellazione di ammassi rocciosi instabili con il metodo degli elementi distinti. *Giornale di Geologia Applicata*, 2, 87-92, DOI: 10.1474/GGA.2005-02.0-12.0038, 2005.
- [19] Bieniawski Z. T. - Engineering classification of jointed rock masses. *Trans S. Afr., Inst. Civ. Engrs*, 15, 335-344, 1973.
- [20] Bruno G. - Caratterizzazione geomeccanica per la progettazione ingegneristica. Flaccovio Dario Editore, Palermo, ISBN 978-88-579-0150-3, 2012.
- [21] Hoek E., Kaiser P. K., Bawden W. F. - Support of underground excavations in hard rock. A.A. Balkema Ed., Rotterdam, 1998.
- [22] Hoek E. & Brown E. T. - Empirical strength criterion for rock masses. *J. Geotech. Engng Div., ASCE 106 (GT9)*, 1013-1035, 1980.
- [23] Ministero Infrastrutture e Trasporti, DM 17 Gennaio 2018 - Aggiornamento delle «Norme tecniche per le costruzioni». *Gazzetta Ufficiale della Repubblica Italiana*, 42, 2018.
- [24] Ambraseys N., Smit, P., Sigbjornsson R., Suhadolc P. and Margaris B. - Internet-Site for European Strong-Motion Data, European Commission, Research-Directorate General, Environment and Climate Programme, 2002.
- [25] Ambraseys N. N., Douglas J., Rinaldis D., Berge-Thierry C., Suhadolc P., Costa G., Sigbjornsson R., Smit P. - Dissemination of European strong-motion data, Vol. 2, CD-ROM Collection, Engineering and Physical Sciences Research Council, UK, 2004.
- [26] Iervolino I., Galasso C., Cosenza E. - REXEL: computer aided record selection for code-based seismic structural analysis. in *Bulletin of Earthquake Engineering*, n.8, 339-362, 2010.
- [27] SeismoSignal_2018 rel.1 - Earthquake Engineering Software Solution. SEISMOSOFT Ltd., Pavia, 2018.
- [28] Barbero M., Barla G., Demarie G. V. - Applicazione del Metodo degli Elementi Distinti alla dinamica di mezzi discontinui. *Rivista Italiana di Geotecnica*, 3, 2004.